EUROPEAN ORGANIZATION FOR NUCLEAR RESEARCH

CERN-PPE/93-169
6 September 1993

In-Beam Experience from the CERES UV-Detectors: Prohibitive Spark Breakdown in Multi-Step Parallel-Plate Chambers as compared to Wire Chambers

R. Baur[a], A. Drees[a], P. Fischer[a,1)], Z. Fraenkel[b], P. Glässel[a], H. Klein[a], A. Pfeiffer[a], A. Schön[a], A. Shor[b,2)], H. J. Specht[a], V. Steiner[b], I. Tserruya[b], Th. S. Ullrich[a]

[a] Universität Heidelberg, Germany[3)]
[b] Weizmann Institute, Rehovot, Israel[4)]

Abstract

The UV-detectors of the CERES/NA45 experiment were originally conceived as parallel-plate counters with two-step amplification, an intermediate gate-electrode pair, and a final drift stage towards a pad electrode. Operated in beams of a few 10^6/burst protons or ^{32}S-nuclei at 200 GeV/u, this scheme was found to suffer from excessive spark rates, even in the gated mode. The origin of the sparks is quantitatively explained by event-correlated slow secondary particles, creating avalanches above the critical threshold of $\sim 10^8$ charges at the required gain of a few 10^5. This lack of sufficient dynamic range is also present in other schemes proposed in the literature; it severely limits the use of large-area parallel-plate counters for single-electron detection in a realistic high-energy physics environment. Possible improvements resulting from resistive anodes instead of metal meshes are also discussed. The spark problem of the CERES UV-detectors was solved by introducing wire amplification as the last stage. Laboratory tests showed a large increase in the dynamic range, due to a strong reduction (by factors of at least 20 – 30) of the net gain of the wire plane for high input charges via space-charge limitation. The residual spark rates of this scheme are lower by orders of magnitude and quite acceptable even for ^{32}S-beams; gating was found to be unnecessary.

to appear in the Proceedings of the First Workshop on RICH Detectors, Bari, Italy (1993)

---

1) now at Universität Bonn, Germany
2) now at Soreq Nuclear Research Center, Yavne, Israel
3) supported by BMFT under grant 06HD525I
4) supported by Minerva and the Kadoorie Family Endowment Fund

1 Introduction

Ever since the double-RICH concept of the CErenkov Ring Electron Spectrometer CERES was first proposed, the discussion of the options for the UV-detectors centered around the conflicting goals of high single-electron detection efficiency, low sensitivity to UV-photon feedback and sufficiently low spark breakdown rates. The feedback problem was solved by selecting two-step multiplication [1] rather than a cloison solution around wires. Prototyping started with low-pressure chambers so as to minimize the dE/dx-signals from traversing charged particles. The first prototype [2], operated with a 80% C_2H_6 / 20% Ar / 34° TMAE mixture at 40 Torr and was composed of a parallel-plate avalanche counter (PPAC) as the preamplifying element and a multi-wire proportional counter (MWPC) with xyu-readout as the terminal element. It already showed the very high gains of up to $> 10^8$ reached in laboratory tests [3] to be by far unobtainable in a realistic high-energy beam environment (in this case a 3 – 5 GeV/c electron + pion test beam from the CERN PS). The next generation of prototypes consisted of two PPAC stages with an intermediate gate-electrode pair, maintaining the low-pressure operation. Both an optical readout [4] and a pad readout [5] were investigated. Using the gated mode to suppress as much as possible spark breakdown triggered by the (uncorrelated) γ and electron radiation environment, the chambers could be operated at gains of up to a few 10^6, but still only at the expense of quite high spark rates considering the small size of the test detector (0.04 m^2).

The final proposal for the CERES experiment [6] was based on this prototype development, selecting the intriguingly simple optical readout with the high gain requirement of a few 10^6 for RICH1 (size 0.42 m^2), and the more complicated pad readout with the more modest gain requirement of a few 10^5 for RICH2 (size 2.8 m^2). Some laboratory tests continued, however, studying in particular the spark breakdown due to γ-ray sources of known strength. It was then recognized that sufficiently slow electrons (with energies of a few keV) could create of order 100 primary charge carriers in a conversion gap of a few mm at 40 Torr, exceeding the critical threshold of $\sim 10^8$ charges for breakdown at a gain of a few 10^6. Detailed estimates [7] led to some quantitative understanding of the observed spark rates and to the conclusion that the maximum gain would have to be restricted to at most a few 10^5 for reasonably safe detector operation in the anticipated event-correlated radiation field (where the gated mode would not help). The optical readout for RICH1 was therefore replaced by pad readout, accepting the complication of the tiny pads (pitch 2.7 × 2.7 mm^2) and the associated miniaturized electronics. At the same time, the low-pressure operation was given up in favor of a 1 atm. He / 6% C_2H_6 / 0.5% TMAE mixture at 50°, accepting the slight increase in dE/dx-signals, but greatly easing the mechanical problems connected with the UV-detector windows. With these changes, the experiment was prepared and installed during 1989/90.

Once the first ^{32}S-beam of 200 GeV/u was switched on in mid-1990, it came as a shocking surprise that the spark rates in both UV-detectors were on an absolutely prohibitive level, although the lowered gain requirements of only a few 10^5 had seemingly been so safe and conservative. Detailed investigations followed, and the origin of the sparks was finally traced back to event-correlated slow secondary hadrons (mostly protons), created in hadronic showers within the material surrounding the experiment. The UV-

detectors were then modified in 1991 by introducing a MWPC as the last stage. Since then, the spark breakdown problem is completely cured, both for proton and for heavy-ion beams, and gating is found to be unnecessary. Based on accompanying laboratory tests, the dramatic spark rate difference between a multi-step MWPC and a PPAC can be understood as a corresponding strong difference in dynamic range: For large avalanche sizes in a MWPC, space charge-effects *limit* the gain, while in a PPAC they *enhance* the gain (ultimately triggering the streamer mechanism).

Ironically, the switch to a multi-step MWPC not only iterated the first prototype [2], but also employed a scheme described already before in the literature on Cherenkov ring imaging [8, 9], including the use of a He/C_2H_6/TMAE mixture [9]. The large difference in practical behavior between a MWPC and a PPAC was, however, not documented before, due basically to a lack of large-scale experience and proper comparison data under beam conditions. Because of the general importance of this topic, we have chosen to present it in this separate paper, following a much more comprehensive description of the CERES RICH detector system and its performance elsewhere in these proceedings [10]. The main purpose of the paper is to illustrate in detail and quantitatively

(i) why a large area multi-step PPAC is restricted to gains of less than 10^4 in a realistic high-energy physics environment, making it essentially unusable for single-electron detection,
(ii) why other proposed PPAC schemes including single-step amplification without any conversion gap may also encounter problems,
(iii) why certain improvements could be obtained from the use of highly *resistive* anodes instead of metallic ones,
(iv) why a large-area multi-step MWPC in contrast to all PPAC schemes does allow safe gains of up to a few 10^5, due to gain compression- (or dynamic range expansion-) factors of at least 20 – 30.

All *technical* details of the UV-detector schemes like mesh planes, wire planes, pad planes, windows etc, are also not described here, but contained in ref. [10] and a forthcoming more detailed paper.

2 The two-step PPAC scheme

The original electrode arrangement of the two UV-detectors brought into operation in 1990 is shown in Fig. 1. The Cherenkov photons enter through the CaF_2 resp. quartz window and are converted into photoelectrons in the 15 mm deep conversion gap. The electrons then drift to the preamplification gap, consisting of two parallel meshes. A large fraction of each electron avalanche ($> 90\%$) is transmitted and drifts through a double transfer gap, split by a pair of two parallel meshes which can be used for gating (application of a pulse of 150 V to the normally back-biased mesh pair). The transferred part of the avalanche is further amplified in a second amplification gap, consisting again of two parallel meshes, and then fed through a final transfer gap onto the detector back plane. This plane contains a resistive layer with about 130 $M\Omega/\Box$ (Abatron), an insulating glass fiber epoxy layer of well-defined thickness, and an array of about 50 000 square pads with a pitch of 2.7 resp. 7.6 mm.

The readout principle is novel and was not yet developed for the original CERES proposal. The electrons drifting through the last transfer gap induce negative charge signals on the pads corresponding nearly to the *full* avalanche size, i.e. at the gas gain M a factor of order $\ln M = \alpha d$ (α Townsend coefficient, d last PPAC gap) is gained compared to anode pads viewing directly the multiplying gap. The time constant for charge motion in the resistive layer is large compared to the electron drift time in the gap; the layer is thus "transparent" for the signals [11]. Formation of the charge signals occurs by integration of the current signals in the pad readout electronics. Since the drift of the electrons is stopped on the resistive layer, the current integration is incomplete, leading to non-zero charge signals on neighboring pads not centered at the avalanche position. This can be used for interpolation, by choosing as an optimum the thickness of the dielectric layer such that the width of the charge signal distribution is about equal to one pad (FWHM). An essential function of the resistive layer is to fix the DC-potential of the last electrode. The scheme thus allows to keep both the pads with the front end electronics and, at the same time, the detector entrance window at ground potential.

With beam on, the RICH detectors showed beautiful rings with the expected number of UV-photons (implying a photo-electron efficiency of $> 90\%$ at a gain of $2 \cdot 10^5$), the expected single-hit resolution (limited essentially by the chromatic aberration of the CH_4 radiator gas), and very low background. However, the spark rates were very much higher than anticipated and, in fact, completely prohibitive for any efficient operation. Systematic data on the spark probability per triggered interaction as a function of the summed voltage change of the two multiplying gaps or, equivalently, the total effective gas gain ($2 \cdot 10^5$ being the reference point) are shown in Figs. 2 and 3 for the two detectors UV-1 and UV-2, resp. They were taken with 200 GeV/u ^{32}S-beams at average beam rates of $2.5 \cdot 10^6$/4 s burst on Pb-targets of 1% and 5% interaction length, choosing various gating conditions and selecting for the gated mode a fixed average multiplicity density of 70 charged particles per unit rapidity. Maximum values of 4% and 20% for UV-1 and UV-2, respectively, are observed at the required gain of $2 \cdot 10^5$, which is equivalent, for the necessary trigger rates of $\geq 50\,000$/burst, to fictitious spark rates of ≥ 2000 and 10 000/burst, resp. These are, of course, not realized; instead, a dead time of > 100 ms exists after each spark to recharge the large electrode capacities, implying effective detector live times of less than 1% – an unacceptable situation.

The untriggered data, corresponding to either gate open (DC) or gate closed, should not be read off as spark *probabilities*, but rather as spark *rates* relative to those in gated mode (obtained by multiplying the ordinate with 25 000/burst), since no trigger is defined. The rates measured with the gate open are higher by a factor of 5 – 10, reflecting the difference between the total target interaction rate (plus any "upstream" interactions) and the trigger rate. The rates measured with the gate permanently closed, though also subject to the overall radiation, are lower by factors of 50 – 100 than those of the gated mode. However, the residual level is still surprisingly high. Such sparks occur in *individual* PPAC gaps, which are operated at gains of only 1000 – 2000, requiring very large primary charge densities indeed to create any breakdown.

The excessive spark probabilities found in-beam are predominantly associated with genuine target interactions. This is not only clear from the large difference between the triggered and the gate-closed data, but directly observed as a proportional change of the

gated-mode spark probabilities with the event multiplicity selected in the trigger. The problem is therefore *not at all specific to the use of heavy-ion beams* with their particularly adverse conditions. Indeed, a similar systematic investigation done in early 1991 with 450 GeV/c protons on heavy targets at beam rates of also a few 10^6/burst showed gated-mode spark probabilities of 0.6% and 3% at the gain of $2 \cdot 10^5$ for UV-1 and UV-2, resp., lower by a factor of about 7 than the corresponding ^{32}S-beam values and thus roughly consistent with the lower charged multiplicity density in the trigger (6 vs. 70), but still implying detector live times of only a few percent. The data further show an identical exponential decrease with the summed voltage change in the detectors and similar relative differences to the gate closed rates as compared to ^{32}S, all pointing to the same physical phenomena underlying the event-correlated spark breakdown.

As investigated recently in a very systematic way [12], but in principle known since many years [13], two quite different breakdown mechanisms can occur in a PPAC. The first one, operating on slow time scales of many μs, originates from photon feedback and sets in at $\eta M > 1$, where η is the rate of secondary photoelectrons per electron in the initial avalanche, and M the gas gain. Since a sufficient amount of quencher gas (C_2H_6) is used in our case, and since the particular problems associated with TMAE are solved by subdivision of the gain into well separated stages, this mechanism can be ruled out. The second one, operating on fast time scales of at most a few 10 ns delay, is mediated by space-charge build-up which locally, between the negatively charged front of the Townsend avalanche and the positive anode, *increases* the externally applied field to a point that an excessive gain is reached and an anode streamer as a precursor to the final breakdown is formed. The critical limit for the onset of the fast mechanism is given by $n_0 M \geq 10^8$, where n_0 is the primary ionization charge contributing to the multiplication process *within the dimensions of the avalanche.* For $n_0 = 1$, this is consistent with the 50-year old "Raether criterion" $\alpha d = \ln M \simeq 20$ [14]. Recent systematic data [12] confirm the near independence of the value 10^8, within a factor of 2 up or down, on the chamber gas, the quencher type and fraction and the gas gain M (varying n_0). Our own laboratory investigations over the years, predominantly concerned with He-mixtures, are also consistent with 10^8, although numbers as low as $3 - 4 \cdot 10^7$ have sometimes been observed. It should be stressed (in contrast to a MWPC, see below) that the multiplication remains strictly linear in charge, i.e. independent of n_0 right up to the sparking limit, defining thereby the dynamic range in very precise terms [12]. It is the fast mechanism then, which causes the high spark rates observed in-beam; this was directly verified experimentally by correlating the time of breakdown with the event trigger.

The discussion of the physical origin of the sparks is now reduced to a discussion of event-correlated particles which deposit a primary ionization of $n_0 \geq 10^8/M$, e.g. ≥ 500 electron-ion pairs at a gain of $2 \cdot 10^5$, in the conversion gap. A comparison of the spark rates between UV-1 and UV-2 shows a difference of a factor of 5, roughly consistent with the difference in total *area* (factor of 6.5), but not at all compatible with the solid angles viewing the target which are nearly identical. This fact, together with the required high ionization density far above the relativistic minimum and the large absolute numbers (the UV-counters are placed *upstream* of the target, see Fig. 1 in ref. [10]), essentially rules out primary particles produced in the target, but points instead to secondary particles of later generations connected with the tails of electromagnetic and hadronic showers. Such

showers occur in the material of the spectrometer itself, but also in the concrete blocks surrounding it; ultimately a nearly isotropic, but still event-correlated low-energy γ and neutron field is created which can provide an area-proportional flux of background to the detectors. The obvious charged particle candidates are therefore low-energy electrons and low-energy protons.

Great care has been taken to make a correct estimate of the ionization density associated with these particles. It is clearly not the often-cited number of primary ionization *clusters* which counts in this case, but rather the total ionization. The specific energy loss for the different gas mixture components has been taken from the usual tables [15], converting it to specific ionization by using the following values for the average energy per ion pair: 29.5 eV for He, 24.6 eV for C_2H_6 [16] and about 24 eV for TMAE. Note that the value of 41.3 eV valid for pure He [16] is lowered by an asymptotic factor of 1.40, if an admixture of only a few 10^{-4} of a molecular gas is added [17], due to an efficient energy transfer from excited metastable states in He (Penning effect). The minimum specific ionization loss in He + an admixture of a few 10^{-4} at STP is therefore 11.6 ion pairs/cm, much higher than the literature value of 4.2/cm ionization *clusters* in pure He [18]. For the gas mixture actually used in the CERES detectors, 94% He + 6% C_2H_6 + 0.5% TMAE (40° satur.) at 50°C and 0.94 atm. (Geneva height), a minimum ionization density of $(8.7+6.1+1.2) = 16$/cm and thus a total ionization n_0^{min} of 24 for a relativistic particle traversing the 15 mm gap at right angles is obtained. In-beam, such particles are seen; they are not critical, but somewhat disturbing for the pattern recognition ("localized clusters"). In considering the other extreme, the maximum ionization n_0^{max} which can be deposited by a particle in the gap, electrons and protons have to be treated in a different way. Electrons follow the specific energy loss à la Bethe-Bloch right down to kinetic energies in the keV region. On a given distance therefore, the maximum deposition is reached if the electron is just stopped. Using range-energy relations [15] with proper interpolation between the constituents, $n_0^{max} \simeq 440$ is obtained for electrons of about 12 keV traversing the 15 mm gap so as to accumulate all primary charge within the lateral dimensions of an avalanche ($\sim$ 2 mm FWHM due to diffusion). Electrons with both smaller and larger kinetic energies deposit less. If, however, the electron direction is parallel to the gap plane, $n_0^{max} \simeq 120$ (energy 3.3 keV) over the 2 mm of the avalanche diameter. For protons, on the other hand, the well-known Bragg maximum rather than the (much larger) stopping energies limit the ionization on a given distance (for $<$ 15 mm), yielding $n_0^{max} \simeq 8000$ for 15 mm (energy 220 keV) and 1200 for 2 mm. It should be stressed that the breakdown limit of 10^8 charges hardly depends on whether the primary charge deposition n_0 is nearly pointlike, or whether it is distributed in space over a long track perpendicular to the electrodes [12].

It appears from the above that electrons in our geometry just happen to be marginally safe towards sparking, even at the full detector gain ($2 \cdot 10^5 \times 440 = 0.9 \cdot 10^8$). They are seen quite frequently, however, running zig-zag at inclined angles through the conversion gap with ranges up to many cm and very large ionization all along the path ("extended clusters"). Their relevance for sparks has been determined directly in the laboratory. In a test detector with a similar He gas mixture but a smaller conversion gap (6 mm, $n_0^{max} \simeq 230$), the spark probability was studied as a function of the gain, exposing the system to a strong γ-ray source nearby. Huge spark rates were seen at high gains which,

followed down to the uncorrelated (low) background level, gave a very well defined onset gain of $(4 \pm 0.5) \cdot 10^5$. With $230 \times 4 \cdot 10^5 = 0.9 \cdot 10^8$, the picture is seen to be consistent [7].

Slow protons, on the other hand, do lead to a fatal limitation, excluding altogether gains above 10^4 for safe operation. At a gain of $2 \cdot 10^5$, a broad range of proton kinetic energies extending to beyond 10 MeV is able to exceed the critical ionization of $n_0 = 500$ in the gap, thereby qualitatively explaining the large observed spark rates. A convincing quantitative verification of the proton hypothesis has been made in the following way. During the same period (1990) and under otherwise identical conditions, data were taken for both UV-detectors at the very much lower gain of 250, allowing to study the absolute probability and the spectral shape of particles with a very large primary ionization in the conversion gap. Large pulse heights were found indeed, corresponding to n_0-values between about 200 (threshold close to the noise of the pad readout electronics), and 6 000 (limited by statistics). The integrated spectrum content was found to be proportional to the event multiplicity (as in the case of sparks). Assuming the critical avalanche size to be given by $n_0 \cdot M = 10^8$, the residual part of the differential spectrum exceeding the critical condition at a given gain can be evaluated as a function of the gain, resulting in the small star-like points labeled "p spectrum" in Fig. 3. The striking agreement of these points with the directly measured spark probabilities, both in absolute magnitude and in shape, implies that the particles responsible for the spark breakdown have been positively identified. The comparable UV-1 data lack statistics (only 5 events), but this is still enough to confirm consistency in magnitude within the error.

As the last step in the argumentation chain, it would finally be of interest to understand the origin of the observed protons. From the point of view of self-absorption, the mechanism may most plausibly be connected with the event-correlated neutron radiation field mentioned before. Neutrons with energies of 1 – 10 MeV and above penetrate large amounts of material; they may then scatter off hydrogen atoms in the detector material (in particular the epoxy planes) and kick the protons into the sensitive detector volume. To quantify this hypothesis, we have mapped the neutron field with monitors in the whole environment of the experiment, making it accessible to easy detection with a thick Fe brick as a target in the beam. Properly normalized, a value of order 10^{-3} neutrons/cm^2 per interaction was obtained in the region of the UV-detectors. Rough insight into the proton energy spectrum can be gained from a transformation of the energy-loss (n_0-) spectrum discussed above, yielding a shape with a peak around 5 MeV and a fall-off towards 50 MeV by a factor of about 10. With suitable assumptions on scattering cross sections and escape depths, the correct order of magnitude (within a factor of 3) for the observed number of protons is obtained. Such a simple procedure is clearly no proof for the proposed mechanism, but is certainly suggestive.

There should be one final word of caution. According to Fig. 2 and Fig. 3, finite spark probabilities still persist at gains $\leq 5 \cdot 10^3$, where sparks from protons should ultimately have died out. It remains unclear at the moment, whether this is due to fluctuations (most plausibly in the threshold number 10^8 itself), or to some very low level of particles with an even higher ionization density. There may also be a connection to the single-gap sparks which occur, although again with quite low probability, at gains down to even only $1 \cdot 10^3$. Even if the bulk of the spark problem discussed above were to be solved, one would still have to be concerned about these more subtle aspects.

We conclude that the essential part of the spark breakdown observed in-beam with the CERES two-step PPAC scheme is quantitatively understood. We also conclude, from the insight into the origin, that a solution will not be possible by tackling the background, but only by properly tuning the geometry and/or the dynamic range such that low-energy electrons and low-energy protons can in principle be accommodated.

3 Generalization to other PPAC schemes

As long as photosensitive vapors like TMAE or TEA are used, a minimum conversion gap of a few mm will always be required, but the final transfer stage as shown in Fig. 1 can then be kept, assuring the full electron signal from the second stage avalanche and thus a dynamic range of $10^8/2 \cdot 10^5 = 500$. However, protons at the Bragg maximum continue to limit the tolerable gain to at most a few 10^4. On the other hand, all more recent proposals to use PPAC's for RICH detectors in high energy physics experiments are based on highly efficient solid photocathodes (like CsI), coupled directly to a single amplifying stage [19, 20, 21, 22]. This automatically implies a loss in usable electron signal by a factor of $\ln M = \alpha d$, requiring gas gains of $1.5 \cdot 10^6$ to obtain a signal of at least 10^5 (the ion component is slow and therefore usually clipped in the readout electronics). The dynamic range now shrinks to only 70. The counter gas is optimized by choosing either a low pressure hydrocarbon (like 20 Torr i-C_4H_{10} [19]), or He with only small traces of CH_4 or CF_4 quencher [21]. Disregarding the former, which is technically extremely difficult and not so much superior, the thinned He mixture does help somewhat (minimum 11 ion pairs/cm at 20°C). Choosing a gap of only 2 mm [21], the effective layer thickness contributing to the final signal is only about 2 mm/$\alpha d \simeq 150$ μm, leading to n_0^{max} of about 30 and 60 for electrons and protons, resp., traversing the gap at right angles. For particle directions parallel to the gap, the lateral extension of the avalanche controls n_0^{max} as before, yielding now, however, (for 1mm FWHM) the relatively higher values, about 70 and 400 for electrons and protons, resp. By chance, the reduction in n_0^{max} is just about compensated by the reduction in dynamic range. Although the sensitive gas volume and thus the effective solid angle of the detector for densely ionizing background is much reduced compared to the CERES case, a completely safe operation can again only be obtained by restricting the effective electron signal to about 10^4 (gain 10^5). There is no obvious way to recover the lost factor of αd and simultaneously keep the photocathode principle.

We conclude that the maximum usable gain of conventional PPAC schemes may quite generally be severely limited by background in a realistic high-energy physics environment.

4 Resistive anodes in PPAC schemes

If the sole occurrence of sparks can not be prevented, their disastrous effect of unloading a whole m^2 large electrode plane with a subsequent long recovery time can surely be addressed. One could conceive of a number of sectors, or in the extreme a very large number of wires, all separately connected via high-ohmic resistors to the HV-supply, which would then minimize the spark energy and shorten the recovery time. The same

benefit could, more elegantly, be obtained by replacing one of the two metal meshes of an amplifying stage with a mesh composed of highly resistive fibers. The area unloaded by a spark would then remain completely local, analogous to "Pestov counters" [23], in which the "microsparks" deliberately induced by overvoltage between a metal electrode and a high-resistivity glass plate ($> 10^{11}\Omega/\Box$) are confined to areas of several mm^2. Unfortunately, such fiber meshes were not available in 1991, and certain commercial developments in this direction [24] have, to the best of our knowledge, thus far not converged.

To gain some insight into the improvements to be expected from PPAC's with resistive electrodes, we have made systematic laboratory investigations [25] as well as first in-beam tests in early 1991, modifying both UV-detectors of CERES accordingly. The electrode arrangement is shown in Fig. 4, making the best possible use of the already existing meshes and the given dimensions (in particular the depth). The Cherenkov photons convert as before; a photoelectron is preamplified in a first stage, the resulting avalanche drifts, is further amplified in a combined gate/2nd amplification stage, drifts further and is amplified once again in a final stage (the previous last transfer gap), using the resistive Abatron layer with about 130 M$\Omega/\Box$ as the anode. Since the pads now view directly the last multiplying gap, the factor of αd is inevitably lost for the induced electron signals.

Laboratory measurements with this scheme were done using both a ^{55}Fe source and a triggered UV-lamp. It came as a big surprise already from the first tests that the critical charge limit for the onset of localized sparks was not the canonical value of 10^8, but definitely higher. Systematic investigations on Abatron layers in the resistivity region of 20 – 130 M$\Omega/\Box$ (in He) consistently gave values around $7 \cdot 10^8$ [25]; quite recent results on "Pestov glass" with $5 \cdot 10^{11}$ $\Omega/\Box$ (in Ar) reproduce the effect at the even higher value of 10^9 [26]. The origin of such an increase is not yet clear, lacking results from an ongoing investigation of the dependence on resistivity and counter gas. Somehow, a coupling between the beginning anode streamer and the anode surface must exist, decreasing the space charge enhancement of the electric field (partial neutralization of the anode surface charge by electrons arriving early?). Pragmatically, the increase is extremely helpful, roughly compensating the loss factor of αd in the compromise setup of Fig. 4, and giving the full benefit in case of a resistive anode *mesh* followed by a further transfer (as in Fig. 1).

The performance of the 3-step scheme in-beam was unsatisfactory. Limits in the overall efficiency of transfer through the many meshes together with limits in the gain of the final stage (see below) required an overall preamplification gain of the two metal mesh gaps such that their spark rate was only lower by a factor of 100 rather than the required 10^4 relative to the rates of the original set-up. Moreover, the very large microspark rate of the last gap, although anticipated, led to excessive charge-up currents of the resistive anode, due to unnecessarily high total charges associated with the individual microsparks. For the 130 M$\Omega/\Box$ layer, laboratory tests have shown the effective surface area feeding a microspark to be at most a few cm^2 [25]; systematic measurements are presently underway to investigate this as a function of resistivity. For a free gap (as with resistive meshes), an area of 2 cm^2 would correspond to a stored charge of $4 \cdot 10^9$ (gap 4 mm, 1500 V). In the compromise set-up of Fig. 4, however, the local capacity unloading into a microspark is dominated by the backplane of the detector, since the pads connected to the input of

the charge-sensitive preamplifiers are effectively on ground. For UV-1 in particular, with an epoxy layer of 0.6 mm and $\varepsilon = 4$, the true microspark charge is then raised to about 10^{11}, increasing the charge-up current by nearly a factor of 30. The compromise scheme was quickly abandoned.

We nevertheless conclude that the use of highly resistive meshes with the benefits of an increased breakdown threshold and only localized microsparks of small charge may save a PPAC scheme even under unfavorable conditions. Further work along this line may be of interest.

5 The double-PPAC + MWPC scheme

By 1991, several groups both at CERN and at Fermilab had gained experience in running large RICH detectors in real experiments. All except CERES were based on MWPC's. A survey made among some of them, in particular WA89 [27] and DELPHI [28], consistently confirmed the presence of "large signals" (much beyond minimum ionization), but also the absence of any disturbing spark breakdown. It is well known that space charge in the avalanches limits the proportional behavior of wire amplification to a total charge of about 10^6 [29]; above, the further growth is increasingly saturated, implying an effective expansion in dynamic range before the onset of breakdown. It was therefore decided to investigate this particular characteristics of a MWPC more closely in the laboratory and to reconfigure the CERES UV-detectors accordingly, adding a MWPC as the last stage.

The electrode arrangement finally arrived at is shown in Fig. 5, keeping the changes relative to the three-step scheme of Fig. 4 to a minimum. A photoelectron is again preamplified in two consecutive PPAC stages, separated by a gate (which later turned out to be unnecessary); the resulting avalanche is then transferred to the MWPC for final amplification. The MWPC consists of an anode plane of 30 μm wires with a spacing of 2 (3) mm, placed asymmetrically within the slightly widened transfer gap of Fig. 1. The resistive layer has now become a cathode, implying also a change in polarity for the signals induced in the pads behind; fortunately, the readout electronics had been conceived to be bipolar. As in any cathode readout, the width of the charge-signal distribution over neighboring pads, allowing for interpolation, is now governed by the anode-pad separation. With the values of 2+0.6 (4+2.6) mm for this separation (limited in UV-1 by mechanical constraints), the width is increased from the 1 pad (FWHM) of the original scheme (Fig. 1) to 2.0 (1.5) pads, hardly affecting the spatial resolution, but raising the fraction of overlapping photon hits around Cherenkov rings to about 20% [10] (in UV-1).

The laboratory investigations on the gain behavior of this scheme were done in parallel at Heidelberg University [30] and at the Weizmann Institute [31], using small test detectors with electrode arrangements nearly identical to Fig. 5. Symmetric and asymmetric MWPC geometries were used. The counter gas was a mixture of He + 6% C_2H_6 + traces of Ar with and without TMAE. The avalanches were initiated with 5.9 keV X-rays from a ^{55}Fe source, corresponding to a primary charge of 220 electron-ion pairs; the Ar helped to increase the X-ray conversion efficiency. Since the results obtained in all cases were very similar, we present here the data set measured with TMAE at 33°C and with a symmetrical 3 mm anode-cathode separation in the MWPC [30]. The primary charge could be preamplified over a very large range, using either the second PPAC (with the

preceding transfer gap as a conversion gap), or both PPAC's. Signals were measured with calibrated preamplifiers on 7.6×7.6 mm^2 pads viewing the MWPC and then properly converted to total charge from the wire plane. The preamplified charge entering the wire plane was obtained from calibrated gain curves of the PPAC's, but could also directly be measured by operating the MWPC stage as a transfer gap or as a low-gain third PPAC analogous to Fig. 4 (with the wire plane at the intermediate potential between the entrance mesh and the resistive layer).

The results on the effective gain M_W^{eff} of the MWPC, defined as the ratio of output to input charge, are shown in Fig. 6 as a function of the wire plane voltage for input charges n_0 ranging from 220 to $5 \cdot 10^6$. The anticipated behavior, i.e. increasing saturation of the output charge with either input charge or gain is very clearly borne out, pointing to gain compression factors of > 100 for this particular geometry and gas mixture. A still more transparent way to illustrate both the gain compression and the associated dynamic range expansion is shown in Fig. 7, where the observed total charge from the wire plane is plotted as a function of the product of the input charge n_0 and the asymptotic (low-n_0) gain M_W^0 of the MWPC; the abscissa thus corresponds to the (fictitious) *output charge of a strictly linear system.* Approximate scaling of the data is observed, strongly supporting the hypothesis of space charge effects. Small scaling violations are, however, also visible (and plausible): at a given value of the abscissa, the saturation effects seem to be weakest if the gain M_W^0 is low. In accordance with previous work [29], complete saturation is reached at an output charge of about 10^8. The dynamic range of the MWPC is therefore not defined by the true output charge, but by the limiting fictitious charge, i.e. the highest value along the abscissa which can be reached before the onset of breakdown phenomena. The critical limit $(n_0 M_W^0)_{crit}$ was found to be around $2 - 3 \cdot 10^9$ for this measurement series. It was determined by the occurrence of small localized discharges, associated with current signals on the pads (into 50 Ω) of about 50 mV with a width of about 300 ns, and thus with total charges of a few 10^9; this closely resembles the "limited Geiger discharges" over ~ 10 mm described before in the literature [32]. No value for the critical limit was given in refs. [29, 32]. The general validity of our particular number is not clear to us. It may well be higher; the second measurement series [31], done in a slightly different geometry and without using TMAE, points to values of even $> 10^{10}$. Compared to a PPAC, however, the dynamic range is extended by a factor of at least 20 – 30, possibly > 100.

The in-beam performance of the MWPC scheme turned out to be a real breakthrough. Under identical environmental conditions as before, both UV-detectors could ever since be operated safely at gains of $2 - 4 \cdot 10^5$, with proton- and ^{32}S beam intensities up to 10^7 particles/burst, and with interaction rates of a few percent of that value, *in fact without using the gate.* Even for protons at the Bragg maximum, the critical limit for the onset of local discharges in the MWPC does not seem to be exceeded ($8000 \times 4 \cdot 10^5 = 3 \cdot 10^9$); we have, at least, only very rarely observed events with characteristics resembling discharges. Genuine spark breakdown is now restricted to the two PPAC preamplification gaps, occurring on the level of about 0.5/burst, i.e. $< 10^{-5}$/interaction. Since the total gain after the second PPAC is restricted to $< 10^3$, this is compatible for ^{32}S with the data of Figs. 2 and 3. For protons, the residual level is found to be hardly lower, pointing to occasional upstream interactions of the beam as the most plausible origin for slow shower

particles traversing the chambers.

We conclude that the dynamic range expansion of a MWPC relative to a PPAC of at least a factor of 20 – 30 has been responsible *and decisive* for a safe operation of the CERES detectors.

6 General conclusion

We abstain from repeating what was repeatedly said in the abstract, in the introduction and in the individual subchapters. Potential applicants of PPAC's will have to draw their own conclusions, depending on their situation. We summarize our own personal view after completion of a full circle and two years of happy data taking in one short remark: We will in all future stick to the lovely tolerance of a MWPC.

Figure Captions

Fig. 1 Original layout of the UV-photon detectors: two parallel-plate stages and a final transfer stage. The dimensions in parentheses refer to UV-2.

Fig. 2 Spark probability per trigger in UV-1 vs. summed high-voltage change (referred to a gain of $2 \cdot 10^5$), or total effective gain. For details see text.

Fig. 3 Spark probability per trigger in UV-2 vs. summed high-voltage change (referred to a gain of $2 \cdot 10^5$), or total effective gain. For details see text.

Fig. 4 Resistive PPAC compromise layout of the UV-photon detectors: three parallel-plate stages, the last one with a resistive anode. The dimensions in parentheses refer to UV-2.

Fig. 5 Final layout of the UV-photon detectors: two parallel-plate stages and a final multi-wire stage. The gate is not used. The dimensions in parentheses refer to UV-2.

Fig. 6 Effective gain of the MWPC for varying input charges vs. anode-cathode voltage.

Fig. 7 Final avalanche size in the MWPC (subject to saturation effects) vs. extrapolated charge in the absence of saturation effects. The different symbols label the input charge to the MWPC; they are the same as in Fig. 6.

References

[1] G. Charpak and F. Sauli, Phys. Lett. **78B** (1978) 523

A. Breskin, G. Charpak, S. Majewski, G. Melchert, G. Petersen and F. Sauli, Nucl. Instr. Meth. **161** (1979) 19

[2] A. Drees, P. Fischer, P. Glässel, G. Lamade, H. Ries, E. Schmoetten, H.J. Specht, A. Breskin, R. Chechik, Z. Fraenkel and I. Tserruya, Nucl. Instr. Meth. **A273** (1988) 793

[3] A. Breskin and R. Chechik, Nucl. Instr. Meth. **227** (1984) 24 and Nucl. Instr. Meth. **A252** (1986) 488; and R. Chechik and A. Breskin, Nucl. Instr. Meth. **A264** (1988) 251

[4] A. Breskin, R. Chechik, Z. Fraenkel, D. Sauvage, V. Steiner, I. Tserruya, G. Charpak, W. Dominik, J. P. Fabre, J. Gaudaen, F. Sauli, M. Suzuki, P. Fischer, P. Glässel, H. Ries, A. Schön and H.J. Specht, Nucl. Instr. Meth. **A273** (1988) 798

[5] P. Fischer, A. Drees, P. Glässel, G. Lamade, H. Ries, A. Schön, H.J. Specht, A. Breskin, R. Chechik, Z. Fraenkel, D. Sauvage, V. Steiner, I. Tserruya and R. Horisberger, IEEE Trans. Nucl. Sci. **NS-35** (1988) 432

[6] U. Faschingbauer, M.G. Trauth, J.P. Wurm, A. Drees, P. Fischer, P. Glässel, M. Guckes, D. Irmscher, L.H. Olsen, A. Pfeiffer, H. Ries, A. Schön, H. Sickmüller, H.J. Specht, T.S. Ullrich, E.F. Barasch, A. Breskin, R. Chechik, Z. Fraenkel, D. Sauvage, V. Steiner and I. Tserruya, Proposal to the SPSC, CERN SPSC/88-25/P237 and SPSC/88-40/P237/Add.1

[7] H.J. Specht, internal CERES note No. 36, 1989 (unpublished)

[8] R. Bouclier, G. Charpak, A. Cattai, G. Millon, A. Peisert, J.C. Santiard, F. Sauli, G. Coutrakon, J.R. Hubbard, Ph. Mangeot, J. Mullie, J. Tiohit, H. Glass, J. Kirz and R. McCarthy, Nucl. Instr. Meth. **205** (1983) 403

[9] G. Charpak and F. Sauli, Nucl. Instr. Meth. **225** (1984) 627

[10] R. Baur, A. Breskin, R. Chechik, A. Drees, P. Fischer, Z. Fraenkel, U. Faschingbauer, J. Gläß, P. Glässel, D. Irmscher, R. Männer, L.H. Olsen, A. Pfeiffer, A. Schön, Ch. Schwick, A. Shor, H.J. Specht, V. Steiner, S. Tapprogge, G. Tel-Zur, I. Tserruya and T.S. Ullrich, J.P. Wurm, these proceedings

[11] G. Battistoni, P. Campana, V. Chiarella, U. Denni, E. Iarocci and G. Nicoletti, Nucl. Instr. Meth. **202** (1982) 459

[12] P. Fonte, V. Pestov and F. Sauli, Nucl. Instr. Meth. **A305** (1991) 91

[13] see, e.g., J.A. Rees (ed.) Electrical Breakdown in Gases, McMillan Press, 1973

[14] H. Raether, Z. Phys. **112** (1939) 464; see also J.M. Meek, Phys. Rev. **57** (1940) 722

[15] Review of Particle Properties, Phys. Lett. **170B** (1986)

[16] H.W. Fulbright, in Hdb. der Physik XLV, Springer, 1958, p. 15

[17] W.P. Jesse and J. Sadauskis, Phys. Rev. **100** (1955) 1755

[18] J. Va'vra, Nucl. Instr. Meth. **A323** (1992) 34

[19] S. Kwan and D.F. Anderson, Nucl. Instr. Meth. **A309** (1991) 190

[20] Y. Giomataris and G. Charpak, Nucl. Instr. Meth. **A310** (1991) 589

[21] Y. Giomataris, G. Charpak, V. Peskov and F. Sauli, Nucl. Instr. Meth. **A323** (1992) 431

[22] C. Lu, K.T. McDonald and Y. Zhu, Nucl. Instr. Meth. (1993) submitted

[23] V.V. Parchomschuk, Yu.N. Pestov and N.V. Petrovykh, Nucl. Instr. Meth. **93** (1971) 269; see also Yu.N. Pestov, Nucl. Instr. Meth. **196** (1982) 45, and later references

[24] by Dupont, Wilmington USA

[25] H.J. Specht, internal CERES note No. 52, 1991 (unpublished)

[26] G. Hansper, Diploma Thesis, Heidelberg 1993 (unpublished)

[27] W. Beusch, J. Engelfried, S.G. Gerassimov, J. Heintze, S. Kluth, P. Lennert, S. Ljungfelt, K. Martens, R. Michaels, U. Müller, H. Rieseberg, H.W. Siebert and G. Wälder, Nucl. Instr. Meth. **A323** (1992) 373; H.W. Siebert, private communication (1991)

[28] E.G. Anassontzis et al., Nucl. Instr. Meth. **A323** (1992) 351; M. Davenport, private communication (1991)

[29] see e.g. S. Behrends and A.C. Melissinos, Nucl. Instr. Meth. **188** (1981) 521

[30] H.J. Specht, internal CERES note No. 57, 1991 (unpublished)

[31] I. Tserruya, internal CERES note No. 58, 1991 (unpublished)

[32] F. Sauli, Principles of Operation of Multi-Wire Proportional and Drift Chambers, CERN Report 77-09 (1977)

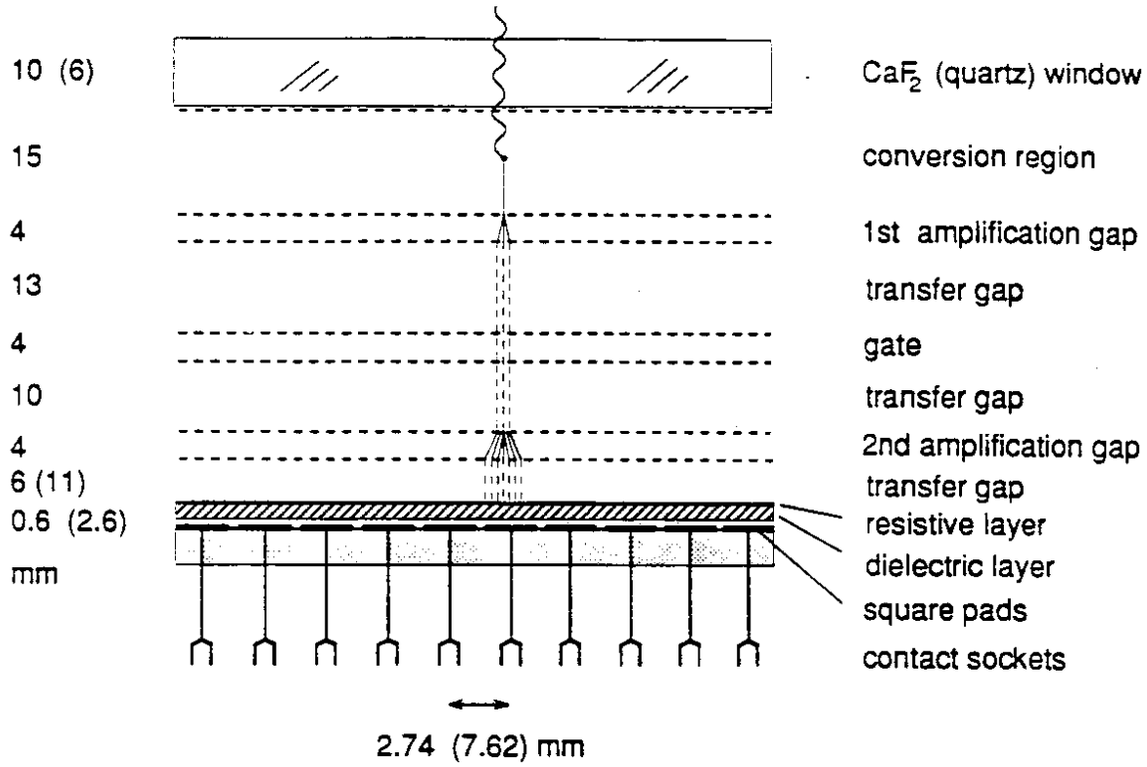
10 (6)
15
4
13
4
10
4
6 (11)
0.6 (2.6)
mm
CaF2 (quartz) window
conversion region
1st amplification gap
transfer gap
gate
transfer gap
2nd amplification gap
transfer gap
resistive layer
dielectric layer
square pads
contact sockets
2.74 (7.62) mm

Fig. 1

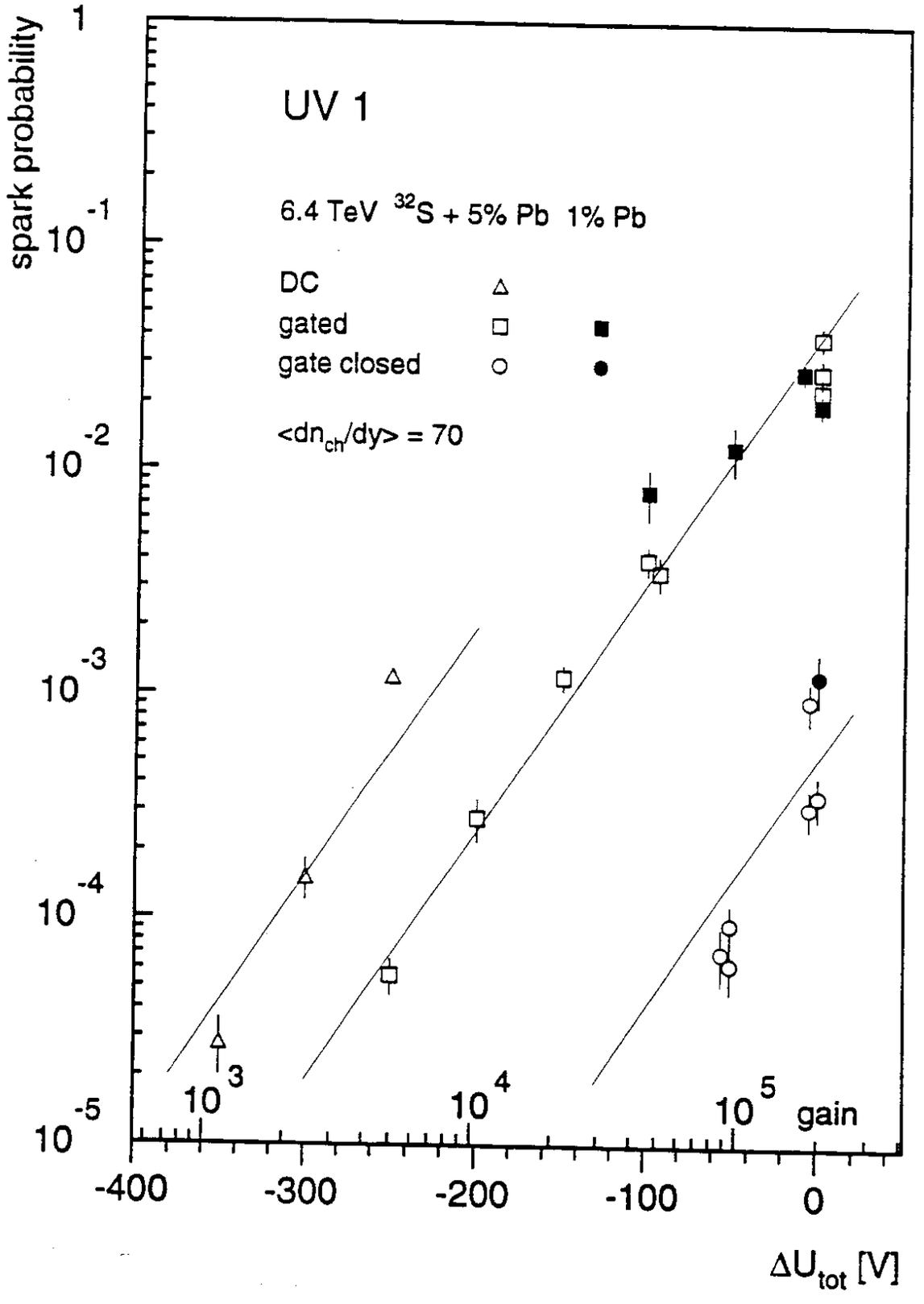
spark probability
1
10^{-1}
10^{-2}
10^{-3}
10^{-4}
10^{-5}
UV 1
6.4 TeV ^{32}S + 5% Pb 1% Pb
DC
gated
gate closed
<dn_{ch}/dy> = 70
10^3
10^4
10^5
gain
-400
-300
-200
-100
0
ΔU_{tot} [V]
uv1−sparks 25.8.93 PG

Fig. 2

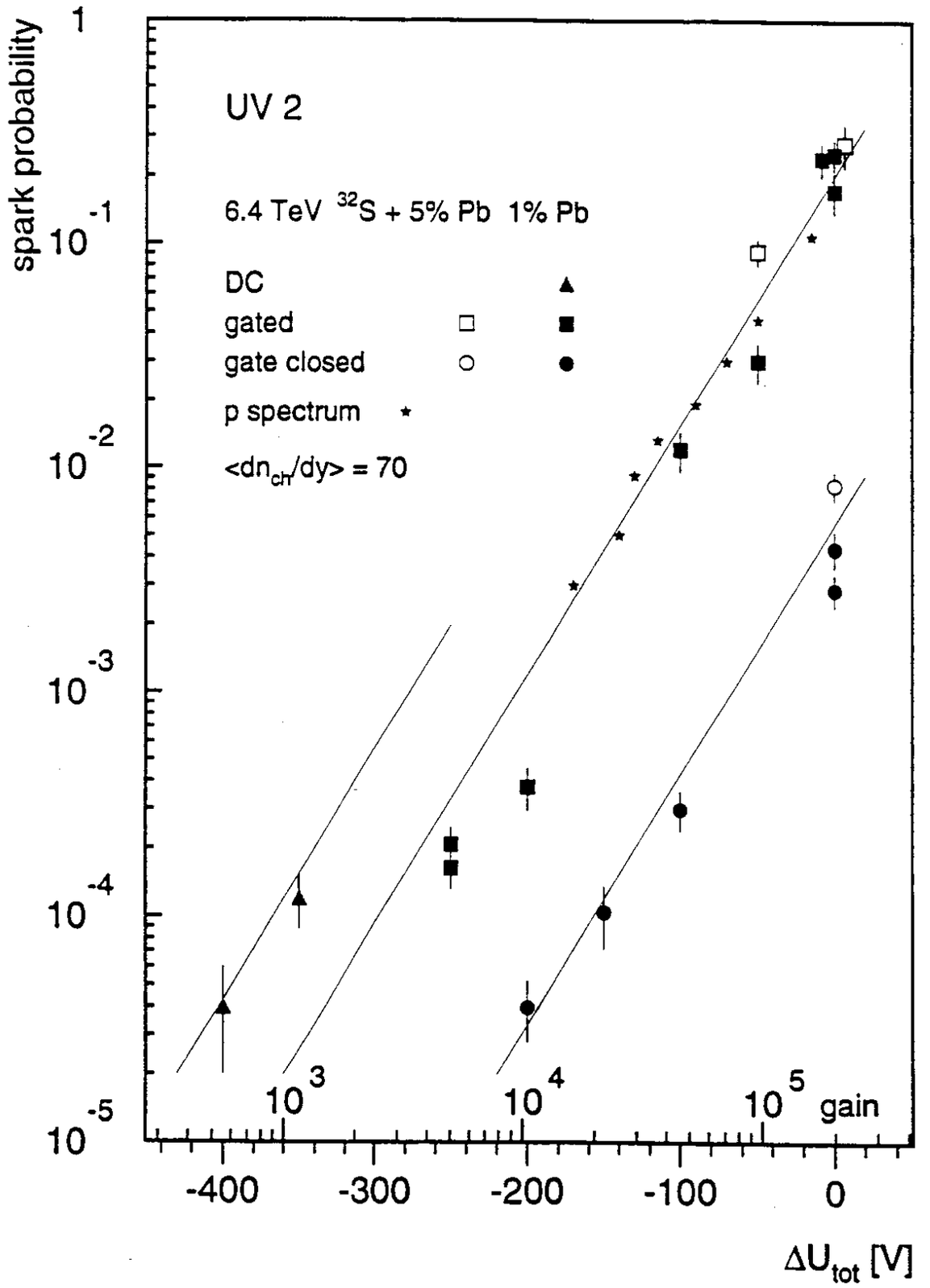
spark probability
1
10^{-1}
10^{-2}
10^{-3}
10^{-4}
10^{-5}
UV 2
6.4 TeV ^{32}S + 5% Pb 1% Pb
DC
gated
gate closed
p spectrum
<dn_{ch}/dy> = 70
10^3
10^4
10^5
gain
-400
-300
-200
-100
0
ΔU_{tot} [V]
uv2−sparks 25.8.93 PG

Fig. 3

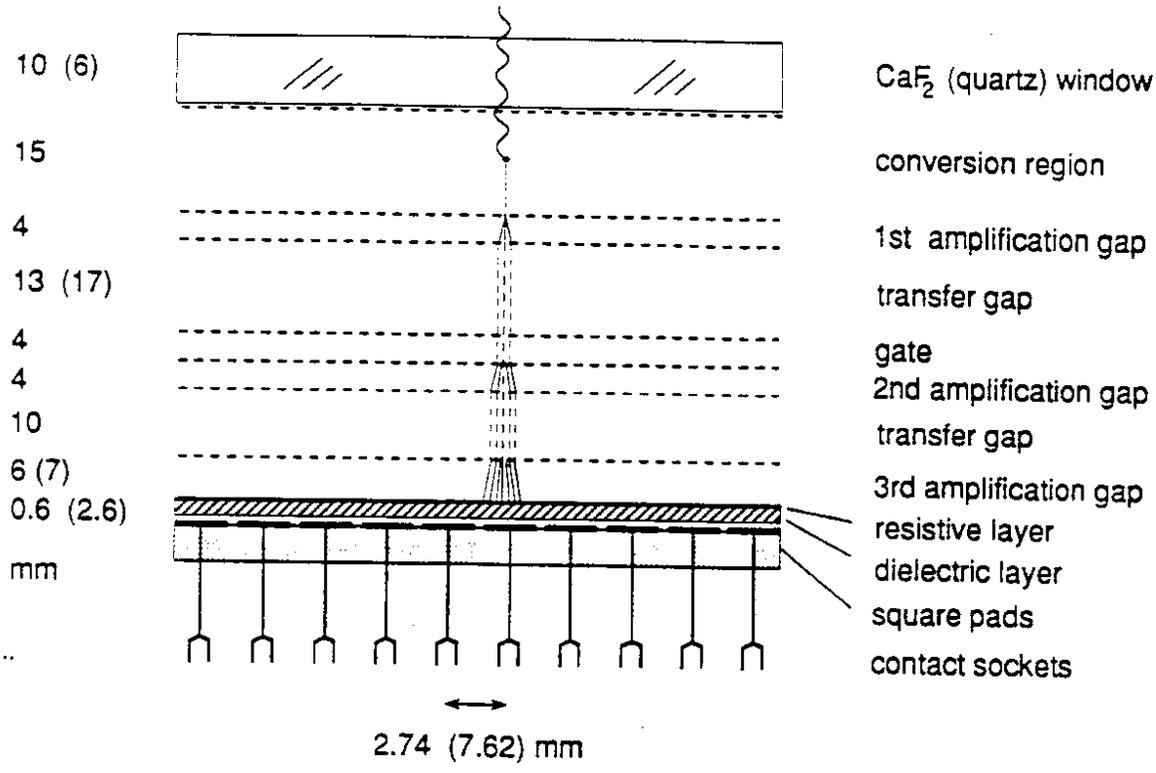
10 (6)
15
4
13 (17)
4
4
10
6 (7)
0.6 (2.6)
mm
CaF2 (quartz) window
conversion region
1st amplification gap
transfer gap
gate
2nd amplification gap
transfer gap
3rd amplification gap
resistive layer
dielectric layer
square pads
contact sockets
2.74 (7.62) mm

Fig. 4

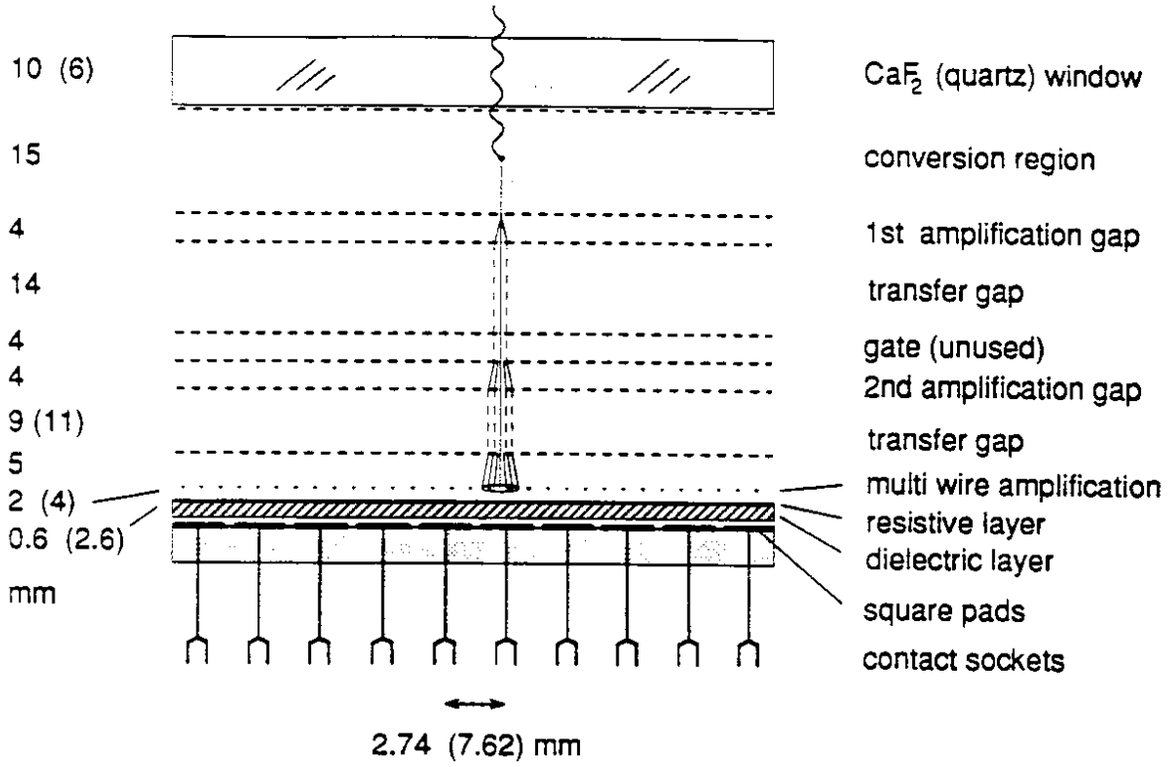
10 (6)
15
4
14
4
4
9 (11)
5
2 (4)
0.6 (2.6)
mm
CaF2 (quartz) window
conversion region
1st amplification gap
transfer gap
gate (unused)
2nd amplification gap
transfer gap
multi wire amplification
resistive layer
dielectric layer
square pads
contact sockets
2.74 (7.62) mm

Fig. 5

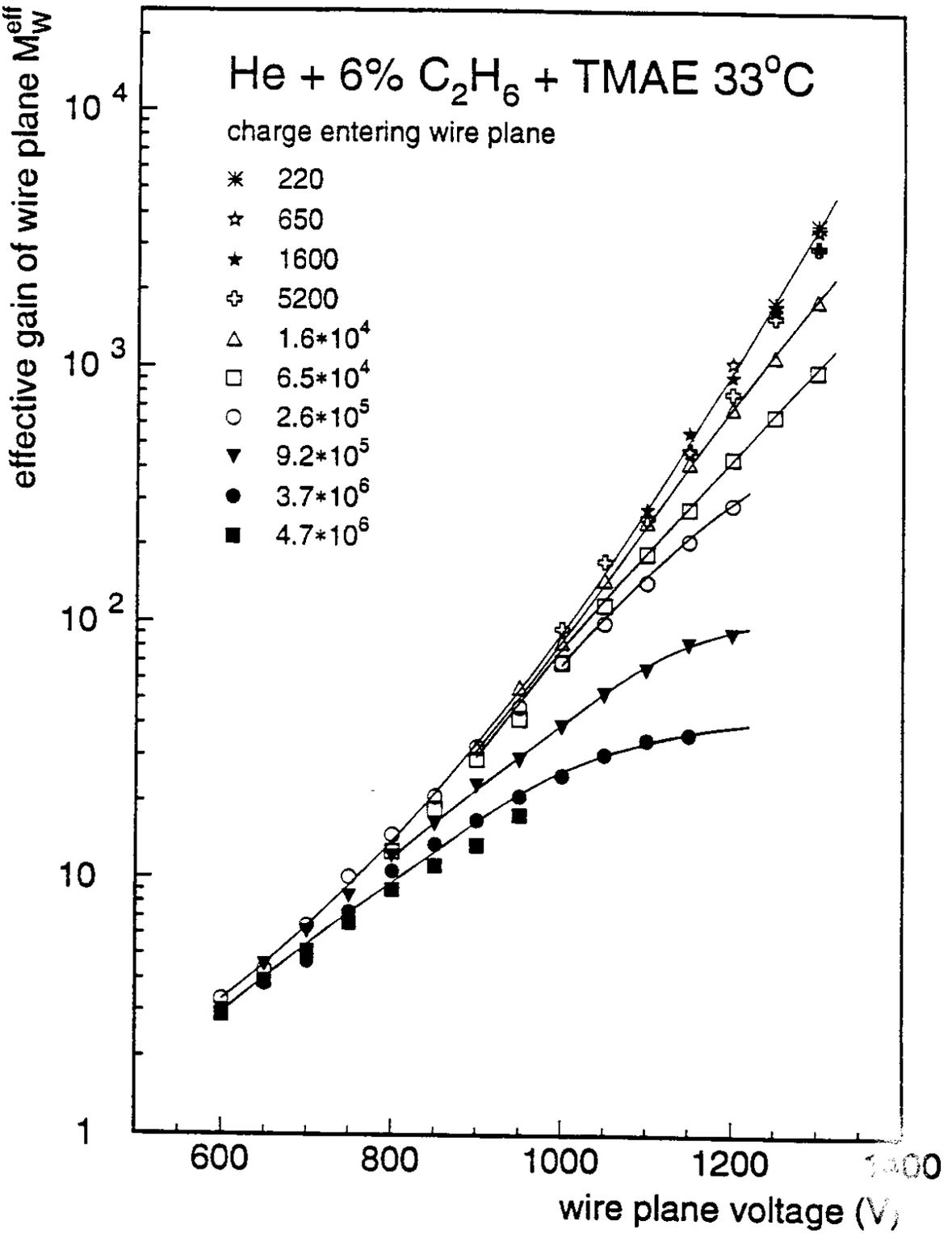

mwgain 24.8.93 pg

Fig. 6

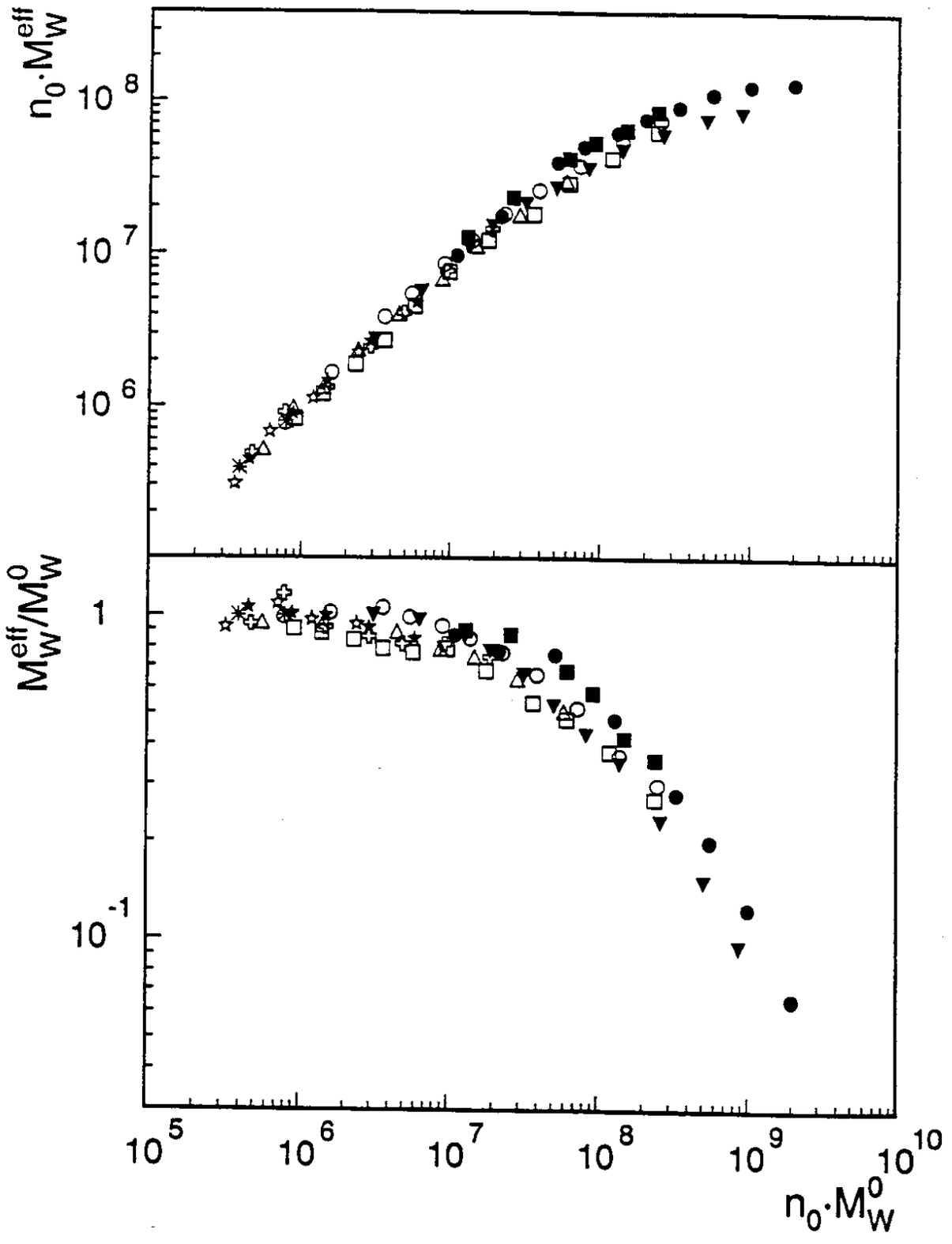

mwcomp 26.8.93 pg

Fig. 7